energy&fuels

pubs.acs.org/EF Article

Fractionation and Characterization of Acidic Compounds of Flowline and Separator Asphaltene Deposits from a Gulf of Mexico Field

Published as part of Energy & Fuels special issue "Celebrating Women in Energy Research".

Priyanka Juyal,* Martha Liliana Chacón-Patiño, and Ryan P. Rodgers

Cite This: https://doi.org/10.1021/acs.energyfuels.4c03528 Read Online

ABSTRACT: Asphaltenes represent the most complex fraction of crude oil, consisting of a diverse range of species with varying sizes, solubilities, aggregation states, structural motifs, and heteroatom contents. In prior work, we identified differences between asphaltenes that deposit in subsea flowlines and those that settle in topside processing facilities. These differences were determined through a variety of techniques, including near-infrared absorbance, bulk elemental analyses, saturates, aromatics, resins, asphaltenes composition profiling, and sequential precipitation using alkanes of different carbon numbers (e.g., C5, C6, and C7). This study extends that research by using high-resolution mass spectrometry to identify molecular-level differences between flow-line and separator deposits. Recent advances in separation methods, such as extrography coupled with high-field Fourier transform ion cyclotron resonance mass spectrometry (21 T FT-ICR MS), have minimized the selective ionization effects of ultracomplex asphaltene samples, thereby enhancing our understanding of their molecular composition, including contributions from both island and archipelago structural motifs. In this work, the two deposit samples were fractionated by extrography and characterized by negative-ion electrospray ionization 21 T FT-ICR MS. Our results reveal significant molecular-level differences between the deposits. The flowline deposit is dominated by species with lower aromaticity and molecular weight, which suggests aggregation behaviors driven by hydrogen bonding and acid−base interactions. In contrast, the separator deposit contains highly aromatic species with higher carbon numbers, indicating a stronger tendency for aromatic stacking and, thus, aggregation. These findings imply that the molecular mechanisms driving subsea deposition differ from those responsible for topside settling. Understanding these distinctions can improve our ability to correlate laboratory results with field data and aid in the development of more effective asphaltene control chemicals.

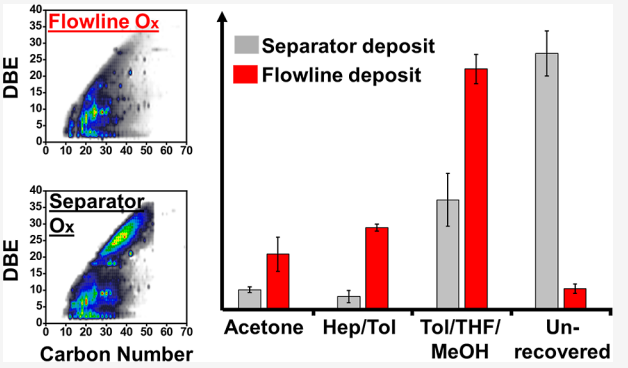

1. INTRODUCTION

Asphaltene deposition is a significant challenge in the oil and gas industry, affecting both upstream and downstream operations. Changes in pressure, temperature, and oil-phase composition during oil production and recovery processes can trigger asphaltene phase separation that adversely affects oil production, transportation, as well as refining. Asphaltene phase separation can cause wellbore and near-wellbore deposition, reservoir fouling, clogging of wells and pipelines, stabilize emulsions, and foul refinery equipment.[1−21] Subsea deposition is a serious concern, with critical repercussions on production economics. Topside settling or sedimentation impact separation processes and optimal production operations. The mechanisms behind asphaltene aggregation, precipitation, flocculation, and deposition continue to be a fascinating scientific challenge and topic of intense debate.[1,4,10,12] The reason for the continued debate is that asphaltenes are arguably the most complex and polydisperse naturally occurring mixture.[22−25] The vague solubility-based operational definition of asphaltenes oversimplifies their chemical intricacy. Therefore, advanced molecular-level diagnostics, such as Fourier transform ion cyclotron resonance mass spectrometry (FT-ICR MS), are vital to understanding the chemical basis of asphaltene-related challenges and developing effective strategies to manage them.[26−31]

Asphaltene characteristics, such as chemical polydispersity and nanoaggregation, contribute to their incomplete diagnosis.[31−35] For instance, nanoaggregation restricts the uniform

Received: July 25, 2024
Revised: October 4, 2024
Accepted: October 7, 2024

https://doi.org/10.1021/acs.energyfuels.4c03528
Energy Fuels XXXX, XXX, XXX−XXX

ionization of asphaltene samples and, therefore, limits the characterization of asphaltenes by MS. Despite such limitations, advances in high-field FT-ICR MS have revealed tens of thousands of unique molecular formulas with various degrees of heteroatom content (e.g., up to five sulfur atoms and five oxygen atoms per molecule, referred to as the O*x*S*y* class), double bond equivalents (a measure of aromaticity, DBE, from 2 to 40), and carbon numbers (from ∼15 to 75). However, routine analysis typically yields highly aromatic and alkyl-deficient compounds that align with the classical "island" model of asphaltene architecture.[31−34] Recent studies that use separations combined with MS for the analysis of crude oils have shown that differences in ionization may greatly challenge asphaltene understanding, as compounds that ionize with greater efficiencies (i.e., highly aromatic species with single core structure) are preferentially observed and mask the detection of poorly ionized compounds in the crude oil/asphaltene sample matrix.[31−36]

We have leveraged an extrography fractionation technique in this study, which selectively targets the removal of asphaltene species that exhibit higher ionization efficiencies (also referred to as monomer ion yields) and, thus, restrict mass spectral characterization of less efficiently ionized species.[31,32] Fractionation enables a comprehensive investigation of asphaltene samples, and when coupled to FT-ICR MS, it is a powerful methodology to allow for insights into molecular features that explain aggregation/deposition trends. The deposits studied here were retrieved from a production facility in a Gulf of Mexico (GOM) well, about 5000 ft in Deepwater GOM. The reservoir pressure and temperature for this well are 20,000 psi and 275−300 F. This well produces from multiple downhole reservoirs and has experienced sharp increases in flowline differential pressure due to rapid asphaltene deposition and has one of the most severe asphaltene deposition issues.[37] Deposition would quickly build up, and before a suitable asphaltene inhibitor program was put in place, the frequency for xylene soaks required for remediation was one soak every 10 days. With 150,000 barrels in deferred production every month, asphaltene deposition greatly impacted this well's production economics.[37] Currently, asphaltene control involves a combination of continuous downhole asphaltene inhibitor treatments and periodic xylene soaks for deposit remediation, as determined by the differential pressure trends. The two deposit samples are from different parts of the system: one is from the subsea flowline, and the other is retrieved from the separator. At the time of sample collection, there was no water production from this oil well. It is expected that the subsea sample is due to deposition, whereas the sample obtained from the separator is due to the gravitational settling of asphaltenic material. Mechanistically, the deposition and settling of asphaltenes are not the same processes. Here, we analyze these samples with various tools and present in-depth characterization results obtained with extrographic fractionation, followed by FT-ICR MS to identify molecular-level dissimilarities between both samples. Diagnoses conducted on these two deposit samples should yield an understanding of unique molecular drivers and chemical bases for subsea deposition vs settling in topside facilities.

2. MATERIALS AND METHODS

2.1. Materials. High-performance liquid chromatography (HPLC)-grade *n*-pentane (*n*-C_5), *n*-heptane (*n*-C_7), acetone (Ace), Tol, THF, methanol (MeOH), and chromatographic grade silica gel (100−200 mesh, type 60 Å, Fisher Scientific) were used as received. Whatman filter paper grade 42 and high-purity glass microfiber thimbles were used for Soxhlet extraction (Whatman, GE Healthcare, Little Chalfont, U.K.).

2.2. Asphaltene Deposit Samples. The two deposit samples were received from a producing field in the GOM, as described earlier. Subsea samples were collected from the flowline, and topside samples were collected from the separator. Deposits did not get exposure to sunlight and were stored in the facility laboratory (offshore) soon after collection and dispatched to our onshore lab. Samples were analyzed and characterized as described in the subsequent sections.

2.3. Deposit Characterization. *2.3.1. Saturates, Aromatics, Resins, and Asphaltene Analysis.* Saturates, aromatics, resins, and asphaltene (SARA) analysis on the two deposit samples was conducted as a first step toward the identification of differences with respect to saturates, aromatics, and polar constituents (resins and asphaltenes). Analysis was conducted according to the procedure reported by Rezaee et al.[38]

2.3.2. Polydispersity Fractionation. Furthermore, to understand the asphaltene polydispersity of the field deposits, a fractionation procedure was conducted to separate each asphaltene deposit sample into four subfractions by sequential precipitation with alkanes of various carbon numbers. In this procedure, the asphaltenes were fractionated based on their solubility in different *n*-alkanes (*n*-C_5, *n*-C_6, *n*-C_7, and *n*-C_8). C_{5-6} asphaltenes represent the lightest fraction of the asphaltenes that are not soluble in *n*-pentane but dissolve in *n*-hexane. The term "lightest fraction" refers to lower molecular weight species, which likely have a reduced tendency to aggregate and a lower content of polar functionalities or heteroatoms. For more details regarding the fractionation procedure, refer to the study by Enayat et al.[39]

2.3.3. Elemental Analysis. Elemental analysis and the H/C ratio for the two samples were also determined.

2.4. Determination of Asphaltene Precipitation Using the Indirect Method for Model Oils Made from the Two Deposits. Flowline deposit and separator deposit samples were dissolved in toluene to prepare model oil nos. #1 and #2, respectively. A concentration of 2 wt % in toluene was chosen for the model oils to match the *n*-C_7 asphaltene content of the parent crude oil. Direct techniques, such as optical microscopy and light scattering methods, are generally used to detect the asphaltene precipitation onset directly. These techniques can only detect the precipitation onset once the size of the asphaltene particles surpasses the specific instrument's detection limit (0.5 to 1 μm). Tavakkoli et al.[21] developed the indirect method with a better detection limit, and it can quantify the mass of precipitated asphaltenes. For more details regarding the indirect method procedure, refer to the study by Tavakkoli et al.[41] In summary, model oil samples were mixed with *n*-heptane (n-C_7) at concentrations of 0−90 vol % of added *n*-C_7. Next, the mixtures were centrifuged for 20 min at 10,000 rpm, which corresponds to 12,740 RCF in the temperature-controlled XIANGZHI benchtop centrifuge model XZ-10. The absorbance of the supernatant liquid (free of asphaltene particles) was measured by a Shimadzu UV-3600 Shimadzu spectrophotometer.

2.5. Fourier Transform Ion Cyclotron Resonance Mass Spectrometry (21 T FT-ICR MS).[42] *2.5.1. Positive-Ion Atmospheric Pressure Photoionization.* Selected samples were diluted in toluene at 100 μg/mL concentration and infused at 50 μL/min into an APPI source. A Thermo Fisher Ion Max APPI source (Thermo Fisher Scientific, Inc., San Jose, CA, U.S.A.) was operated with a vaporizer temperature of 350 °C, a N_2 sheath gas at 50 psi, and a N_2 auxiliary gas at 32 mL/min, which prevented sample oxidation. Toluene is used as a solvent/dopant to increase analyte ionization through dopant-assisted proton-transfer and charge−exchange reactions that are initiated by ionized toluene molecules at atmospheric pressure inside the ionization source in positive-ion mode.

2.5.2. Negative-Ion Electrospray Ionization. Deposit extracts and extrography fractions (generated as described in Section 2.6) were diluted to a final concentration of 100 μg/mL in a 1:1 toluene/methanol with 0.1% of tetramethylammonium hydroxide (TMAH)

https://doi.org/10.1021/acs.energyfuels.4c03528
Energy Fuels XXXX, XXX, XXX−XXX

solution added to aid deprotonation. Samples were ionized by micro-ESI with a needle voltage of −2.8 kV and an infusion rate of 0.5 $\mu g/mL^{-1}$.

Produced ions, via either APPI or ESI, were analyzed with a custom-built hybrid linear ion trap FT-ICR MS equipped with a 21T superconducting solenoid magnet. Instrumentation and technique have been described previously.[42,43] Ions were initially accumulated in an external multipole ion guide and released m/z-dependently.[44] Ions were excited to m/z-dependent radius to maximize the dynamic range and number of observed mass spectral peaks,[44] and excitation and detection were performed on the same pair of electrodes.[45,46] The dynamically harmonized ICR cell in the 21 T FT-ICR is operated with a 6 V trapping potential.[43,47] Time-domain transients of 3.2 s were acquired with the Predator data station, with at least 100 time-domain acquisitions averaged for all experiments.[48] Mass spectra were phase-corrected and internally calibrated with several "Kendrick" homologous series based on the "walking" calibration method.[49] Peaks with signal magnitude greater than 6 times the baseline root-mean-square (RMS) noise at m/z 500 were exported to peak lists, and molecular formula assignments and data visualization were performed with PetroOrg© software.[50] Molecular formula assignments with an error >0.25 parts-per-million (ppm) were discarded, and only chemical classes with a combined relative abundance ≥0.15% of the total were considered.

2.6. Asphaltene Fractionation. The deposits were treated as crude oils and separated into C_5 maltenes, inbetweeners, and C_7 asphaltenes; the method has been described previously.[50,51] Thus, C_7 asphaltenes from the deposits were further separated by extrography. In short, silica gel was dried overnight at 120 °C prior to the adsorption of the C_7 asphaltenes. A total of 100 mg of asphaltenes were dissolved in 400 mL of DCM, placed in a round-bottom flask, and mixed with 10 g of silica gel (10 mg of asphaltenes/g of SiO_2). The mixture was stirred at 1500 rpm under a N_2 flow until complete solvent evaporation. The composite SiO_2/asphaltenes was placed in a Soxhlet apparatus and extracted using the following solvents: Ace, 1:1 Hep/Tol, and 1:1:1 Tol/THF/MeOH, which yielded three fractions from each C_7 asphaltene sample. The method is discussed in detail elsewhere.[30] The fractionation process was performed in triplicate for each asphaltene sample. All of the fractions were dried under nitrogen, weighed, and stored in the dark for future analyses.

3. RESULTS AND DISCUSSION

Table 1 shows the SARA analysis results of the flowline and separator deposits.

Table 1. Results of SARA Analysis for Flowline and Separator Deposits

SARA analysis	flowline deposit	separator deposit
saturates, wt %	47.9	28.7
aromatics, wt %	0.4	1.6
resins, wt %	8.2	8.8
n-C_7 asphaltenes, wt %	43.1	60.4

The flowline deposit presents a higher aliphatic character and has relatively less aromatic, resin, and asphaltene content than the separator deposit. The separator deposit is overall more aromatic, with a significantly higher n-C_7 asphaltene content. This dissimilarity may be attributed to the deposits' polydispersity, which demonstrates that the two field deposits from different locations in the same production facility are not similar in terms of chemical composition. The flowline deposit is attributed to actual subsea deposition phenomena that depend on the net mass of precipitated asphaltenes, their particle size, flow regimes, surface properties, etc. Deposition results from the accumulation of asphaltene mass on the production tubing and flowlines, a phenomenon not entirely understood but has been explained by precipitation, aggregation, advection, and deposition, with fluid flow rates and shear removal of precipitated asphaltenes also impacting net deposition.[1,10,39,40] On the other hand, the separator deposit results from sedimentation or gravitational settling of destabilized asphaltenes carried over by the crude oil in topside processes under a more static environment. Therefore, this subset of precipitated asphaltene would be the fraction that did not deposit subsea or was removed by shear. Progress in understanding asphaltene deposition is challenged due to the intricate chemical nature of asphaltenes.

The results of the asphaltene fractionation of the flowline and separator deposits are revisited in Table 2.[37]

Table 2. Results of Asphaltene Polydispersity for Flowline and Separator Deposits

asphaltene fraction	flowline deposit	separator deposit
C_{5-6} asphaltenes, % of C_{5+} asphaltenes	16.3	9.9
C_{6-7} asphaltenes, % of C_{5+} asphaltenes	7.9	0.0
C_{7-8} asphaltenes, % of C_{5+} asphaltenes	5.9	2.9
C_{8+} asphaltenes, % of C_{5+} asphaltenes	69.9	87.2

Asphaltene fractionation data, shown in Table 2, further showcase the dissimilarities between the two deposits. The separator deposit has a higher portion of the n-C_8 asphaltenes, which are heavier and more unstable, as determined by solubility/stability tests. The impact of asphaltene polydispersity on stability and deposition has been reported by Khaleel et al. with two model oil systems derived from the same crude oil with detailed analysis and testing, where model oil 1 featured more of the lighter asphaltenes, with a lower molecular weight (C_{5-6}) and model oil 2 had more of the heavier asphaltenes (C_{8+}).[40] Model oil 2 was reported to be more unstable, with a lower precipitation onset than model oil 1.[40]

Elemental analysis data are reported in Table 3. The separator deposit analysis yields lower H/C compared to the flowline deposit, which aligns with observations made from SARA and polydispersity analyses conducted on these two samples. These bulk measurements were published by Juyal et al.,[37] and are being revisited here to facilitate the discussion and to lead to our next steps in differentiating the samples at the molecular level.

Table 3. Elemental Analysis of the Flowline and Separator Deposit Samples

	weight %				
sample	carbon (C)	hydrogen (H)	nitrogen (N)	sulfur (S)	H/C
flowline deposit	79.8	9.5	0.8	1.0	1.4
separator deposit	87.3	8.6	0.9	1.2	1.2

The asphaltene precipitation tendency of the crude and model oils prepared with the deposit samples (2 wt % in toluene) was determined by the indirect method for a study that was earlier reported by Juyal et al.[37] Figure 1 revisits the indirect method results at 70 °C and 1 h of aging time for the model oils diluted with n-C_7. In these plots, a drop in the absorbance value indicates precipitation and the subsequent removal of asphaltene particles by centrifugation. The concentration of n-C_7 at which the absorbance value deviates

https://doi.org/10.1021/acs.energyfuels.4c03528
Energy Fuels XXXX, XXX, XXX−XXX

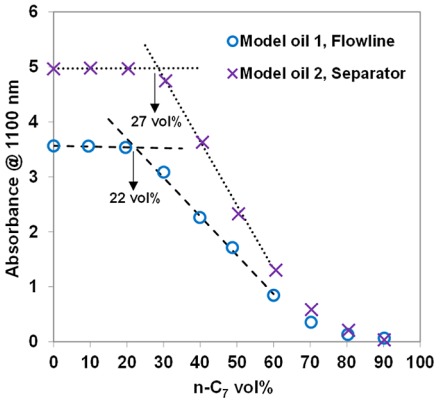

Figure 1. Results of the indirect method at 70 °C and 1 h aging time for model oils #1 (made with flowline deposits) and model oil #2 (made with separator/topside deposits), diluted with C_7. (Data published in Juyal et al.[37])

from the horizontal trend is considered the asphaltene precipitation onset. This concentration is obtained by finding the intersection of two trend lines before and after the onset. The accurate determination of the onset of asphaltene precipitation allows the appropriate selection of the precipitant-to-oil ratio and the determination of the tendency toward asphaltene precipitation and deposition. One interesting observation from the data shown in Figure 1 is the higher absorbance value of the model oil made with the separator deposit than the model oil made with flowline deposits (with the same asphaltene concentration of 2 wt % in toluene). This observation suggests that the separator deposit has higher aromaticity and/or larger aggregates in comparison to the flowline deposit. This discrepancy in optical behavior triggered our interest in a deeper understanding of the molecular-level differences between subsea deposition and settling in topside facilities.

3.1. Positive-Ion APPI 21 T FT-ICR MS. Asphaltenes are ultracomplex mixtures of tens of thousands of different chemical species. Although high/ultrahigh resolution MS is an ideal tool to conduct molecular-level diagnostics on complex hydrocarbon samples, heterogeneous aggregation of asphaltenes significantly impacts the ionization efficiencies and thus limits characterization. As discussed earlier, in mass spectrometric analysis, the most aromatic species are often preferentially observed by direct infusion APPI MS.[29,31,34,52−58] Figure 2 shows the compositional data derived from + APPI 21 T FT-ICR MS for the entire deposit samples. Figure 2 (top) shows the class distribution, whereas the bottom panel features isoabundance contoured plots of DBE vs carbon number for hydrocarbons (class HC, species with no heteroatoms) and the O_1 class, two of the most abundant compound classes detected. Clearly, the results indicate that the APPI FT-ICR MS of whole (unfractionated) samples do not offer apparent differentiation between the two deposits. It is imperative to stress again that complex mixtures require special attention due to differences in ionization efficiency between chemical species and, in the case of asphaltenes, their aggregation state.[59] Furthermore, analysis of asphaltenes by MS is especially compromised by the presence of maltenes, which has been observed in exhaustively extracted asphaltene samples with heptane.[60] Even with APPI, thought to be the most suitable ion source for asphaltenes, the most easily ionized compounds are preferentially detected and often do

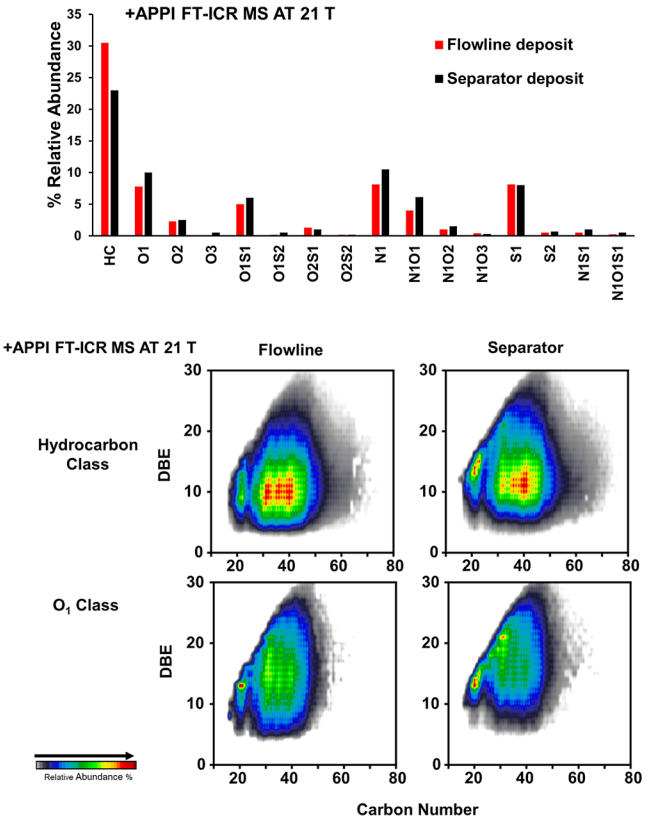

Figure 2. (Top) heteroatom class distributions, derived from positive APPI FT-ICR mass spectra, for the flowline and separator whole deposit samples. Only classes with relative abundances >1% are shown. (Bottom) relative iso-abundance color-contoured plots of DBE vs carbon number for the hydrocarbon and O_1 oxygen class from whole flowline and separator deposit samples.

not reflect the bulk elemental composition of the whole sample. Thus, only those compounds that exist in a nonaggregated state (monomers) are detected in the typical mass range of most commercial mass spectrometers ($200 < m/z < 2000$). Thus, a significant fraction of whole asphaltene samples is not detected by direct infusion MS on unfractionated asphaltenes,[29,31,34,52−60] which also seems to be the case for the flowline and separator deposit samples.

A more comprehensive mass spectrometric characterization can be achieved through the implementation of separation techniques that allow sample fractionation based on the aggregation tendency and polarity, among other molecular properties.[31,61−63] To offset limitations imposed by asphaltene aggregation, in this work we use extrography, which facilitates the selective removal of asphaltene species with high monomer ion yields, allowing better characterization of less efficiently ionized compounds.[31] Silica gel serves as the stationary phase; extraction with Ace, a solvent with dominant dipolar interactions, helps to isolate highly aromatic compounds with dominant single-core (island) structural motifs. Conversely, the Tol/THF/MeOH solvent mixture preferentially extracts multicore (archipelago) structural motifs.[31,63−65] The gravimetric yields for the extrographic fractionation for the flowline and separator deposits are shown in Table 4 and Figure 3.

Removing coprecipitated maltenes from C_7 asphaltenes is critical for their mass spectral analysis, as maltenes ionize with much greater efficiency than asphaltenes. The flowline sample is higher in C_5 maltenes and lower in C_7 asphaltenes,

https://doi.org/10.1021/acs.energyfuels.4c03528
Energy Fuels XXXX, XXX, XXX−XXX

Table 4. Solubility Fractions and Extrographic Fractions Yields Derived from the Separator and Flowline Deposits

average results (triplicates)	solubility fractions (weight %)			extrography fractions from C_7 asphaltenes (weight %)			
	C_5-maltenes	"inbetweeners"	C_7–Asph	Ace	Hep/Tol	Tol/THF/MeOH	unrecovered material
separator	25.9	2.2	68.9	5.0	3.3	27.5	64.2
flowline	38.9	1.3	54	13.9	20.6	60.3	5.3

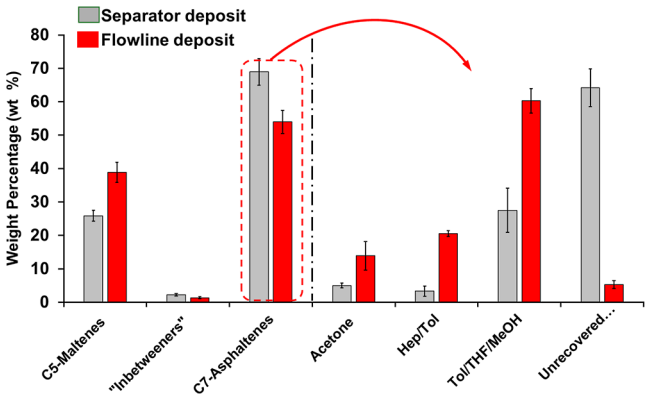

Figure 3. Gravimetric yields for the extrographic fractionation results for the separator and flowline field deposit samples.

suggesting that the subsea deposit features "lighter" species. This observation is qualitatively in line with previously presented SARA composition and polydispersity data derived with sequential extraction with *n*-alkanes for the two field deposit samples (Tables 1 and 2), though not exactly alike due to different methodologies performed at different laboratories. "Inbetweeners" comprise the fraction soluble in C_7 but insoluble in C_5, and both samples present a limited amount of such compositions.

Regarding C_7 asphaltenes, their separation is extended by extrography. A major difference between the two C_7 asphaltene samples obtained from the two deposits is the total mass recovery upon extrography. The separator sample contains significant amounts of unrecovered material, indicating the presence of highly polar species that irreversibly adsorb onto silica gel. Both samples have remarkably different yields for the Tol/THF/MeOH fraction. Furthermore, the results indicate a near-complete recovery (extraction from silica gel) for the flowline deposit sample. Indeed, the high yield of the Tol/THF/MeOH fraction in the flowline sample suggests a significant contribution of archipelago-type species in subsea deposition.

Extrographic separation yielded obvious differences for the flowline and separator deposit samples, emphasizing that for this crude oil, the molecular drivers for subsea deposition may not be the same as the topside settling of asphaltenes. To investigate the molecular level differences, we characterized each solubility (maltenes and "inbetweeners") and extrographic fraction obtained from the deposit samples using negative-ion ESI 21 T FT-ICR MS. ESI was used to facilitate access to acidic polar species, as they have been proposed to have a critical role in adsorption on surfaces (polar interactions), asphaltene aggregation, and emulsion stabilization.[66,67,73,78]

3.2. Characterization of C_5 Maltenes. Figure 4 (top) shows the heteroatom class distribution for C_5 maltenes for the two deposit samples. Combined iso-abundance contoured DBE vs carbon number plots for all N- and O-containing compounds (plots to the left) and for all S-containing species (plots to the right) are shown in Figure 4 (bottom). The heteroatom class distribution graph highlights no significant differences between the two samples. Likewise, the DBE vs carbon number plots for all N- and O-containing classes appear similar. Abundant S-containing compounds with low DBE values (Figure 4) are observed. Those species have been previously reported as "natural" surfactants and may potentially be "sulfonic acids", known for their interfacial activity and contribution to emulsion stabilization.[66,67]

3.3. Characterization of "Inbetweeners" Asphaltenes. "Inbetweeners" are the species soluble in C_7 but insoluble in C_5. They are called "inbetweeners" as they are a solubility fraction between C_5 maltenes and C_7 asphaltenes. Figure 5 (top) shows the heteroatom class distribution for the inbetweeners from the two deposit samples. NO*x* species are the most abundant class for both samples. The DBE vs carbon number plots for all NO*x*- and SO*x*-containing compounds are shown on the lower side of Figure 5. There is no significant difference between the two samples. However, it is highlighted that inbetweeners feature higher amounts of O-containing species, NO*x*, which indicates that the solubility of the studied samples might be ruled by the content of oxygen functionalities. Previous reports on deposits from this field indicate that deposit samples from this field typically exhibit elevated total acid number (TAN) values. For instance, a prior deposit sample showed a TAN of 6 mg KOH/g, compared to a TAN of 0.23 mg KOH/g in the untreated crude oil. This significant difference suggests an enrichment of organic acid species in the deposits, suggesting their involvement in the deposition process.

The following section focuses on analyzing the extrography fractions from the C_7 asphaltenes isolated from the two deposit samples to further explore the molecular-level differences between the two deposits.

The whole deposit sample has not been analyzed by negative ion ESI since, at National High Magnetic Field Laboratory, we have frequently analyzed whole samples alongside their fractions, and we have consistently observed a more comprehensive compositional coverage when integrating information from fraction analysis compared to the analysis of whole samples alone. This trend has been documented across various ionization techniques, including ESI, APPI, and MALDI (Rodgers et al., 2019; Chacon-Patino et al., 2022, 2023).[59−61]

3.4. Extrography Separation: Acetone, Hep/Tol, and Tol/THF/MeOH Fractions. As highlighted earlier, Ace extraction yields a fraction that is enriched with highly aromatic species. Furthermore, Ace is highly selective toward the extraction of small/peri-condensed aromatic ring systems (1−4 fused rings) due to its moderate solvating strength for PAHs.[31,70,71] Previous reports indicate that Ace is suitable for the selective removal of low-molecular-weight asphaltenes with dominant single-core structure (island), petroleum porphyrins, and coprecipitated/entrained maltenes within asphaltene aggregates.[31,72−74] Regarding Hep/Tol, it is the extraction of alkyl-aromatic species, likely a mixture of single-core and

https://doi.org/10.1021/acs.energyfuels.4c03528
Energy Fuels XXXX, XXX, XXX−XXX

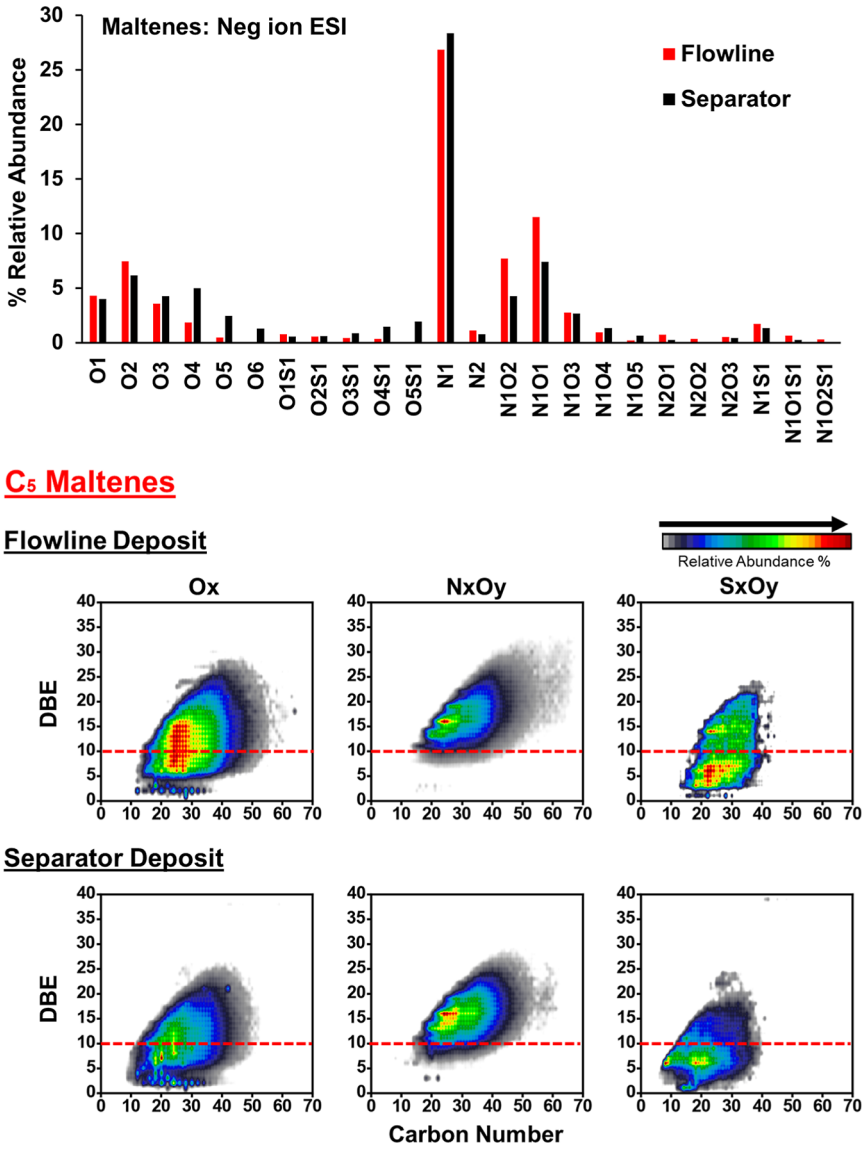

Figure 4. (Top) heteroatom class distributions, derived from negative-ion ESI 21 T FT-ICR MS, for the C_5 maltenes from the flowline and separator deposit samples. (Bottom) combined iso-abundance color-contoured plots of DBE vs carbon number for all O*x* (i.e., O_1, O_2, O_3, O_4, and O_5), N*x*O*y*, and S*x*O*y* species for C_5 maltene fraction for the flowline deposit (upper row) and the separator deposit (lower row).

multicore (archipelagos) structural motifs.[31] Finally, the Tol/THF/MeOH fraction is enriched with multicore species and functional groups capable of hydrogen bonding to the silica gel. As shown in Table 4 and Figure 3, the high yield of the Tol/THF/MeOH fraction in the flowline sample suggests a significant contribution of archipelago-type species, as previous studies have demonstrated that this fraction is typically enriched in multicore or archipelago structures. This has been confirmed through gas phase fragmentation in several samples from diverse geological origins, providing direct evidence of these complex species. The Tol/THF/MeOH fraction is in low concentration in the separator deposit (Table 4 and Figure 3), which features extensive amounts of unrecoverable material, i.e., material that remained irreversibly adsorbed on the SiO_2. We hypothesize that the unrecoverable compounds could be linked to a stronger aggregation, deposition, and fouling tendency.

Figure 6 shows the heteroatom group distribution, derived from negative-ion ESI 21 T FT-ICR MS analysis, for the extrography fractions for the two deposit samples (the flowline deposit is shown to the left, and the separator deposit is shown to the right). Here, the different heteroatom classes are grouped to facilitate data interpretation. For example, N_1O_1, N_1O_2, N_1O_3, etc., are grouped as N_1O_x. The Ace fraction for the two samples reveals no significant differences in the heteroatom distribution; compared to the rest of the extrography fractions, Ace appears to be depleted in the O_x compositions. Conversely, the Hep/Tol fractions have higher amounts of the O_x species, which is more prevalent for the flowline deposit. Notably, the Hep/Tol fraction for the separator deposit reveals heteroatom groups, N_xS_y and $N_xO_yS_z$, that are not present in the flowline sample. Compounds with small aromatic cores, limited content of alkyl side chains, multiple oxygen atoms (O_{3-6}), or combinations of nitrogen and oxygen ($N_{1-2}O_{3-6}$) have been previously reported by Zeng et al. Given their possible structural features, the authors referred to those species as "sticky molecules".[75] It has been suggested that sticky molecules act like "double-sided tape",

https://doi.org/10.1021/acs.energyfuels.4c03528
Energy Fuels XXXX, XXX, XXX−XXX

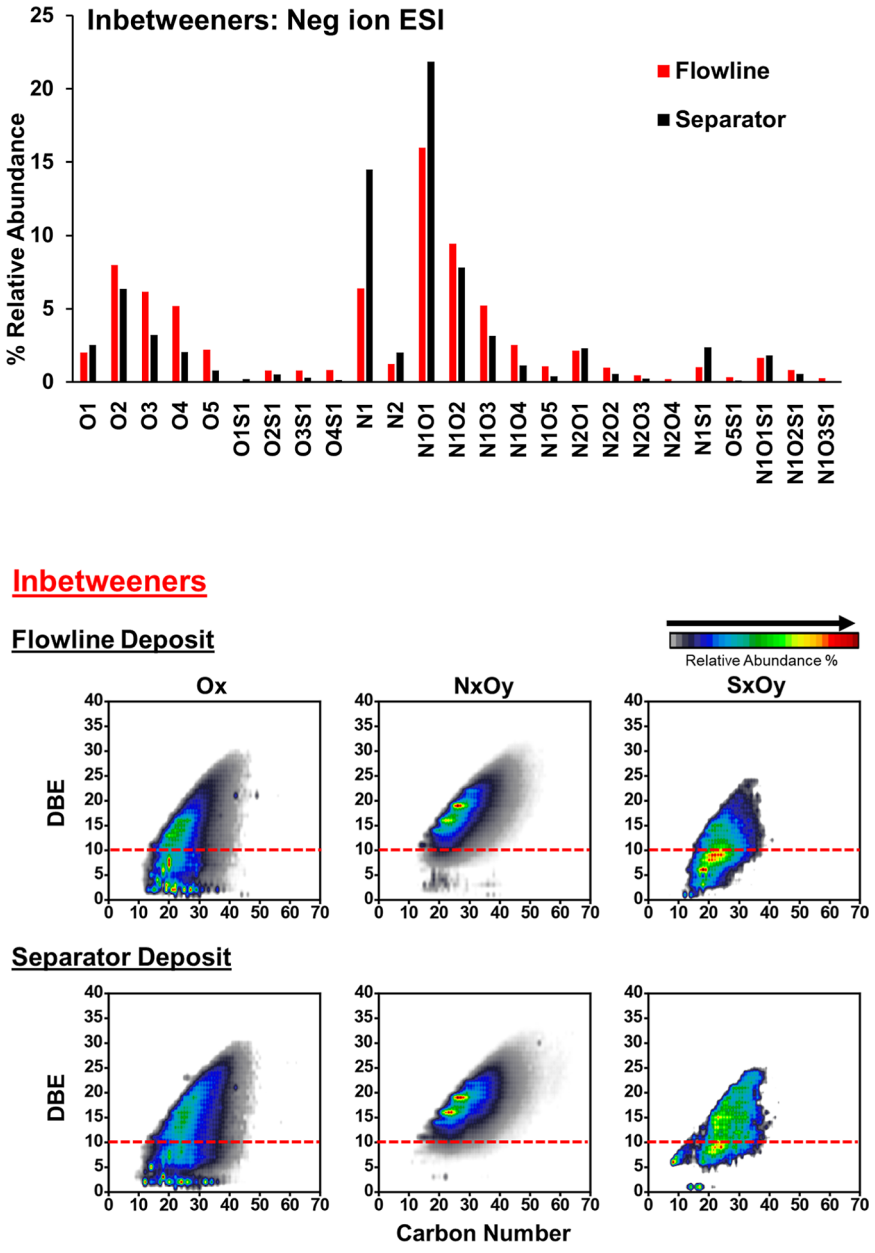

Figure 5. (Top) heteroatom class distributions, derived from negative-ion ESI 21 T FT-ICR MS, for the "inbetweeners" for the flowline (red) and separator deposits (black). Only classes with relative abundances >1% are shown. (Bottom) iso-abundance color-contoured plots of DBE vs carbon numbers for all O*x*, N*x*O*y*, and S*x*O*y* species for the "inbetweener" fraction for the flowline deposit (upper row) and the separator deposit (lower row).

which helps to strongly bind the destabilized asphaltenes to the rock surface. It is important to highlight that species with a high oxygen content have also been observed frequently for other deposit samples from the GOM. This fact highlights the role of acidic, oxygen-containing species in asphaltene deposition on topside facilities. Finally, the Tol/THF/MeOH fractions also reveal a high abundance of O_x species for both deposit samples.

Figure 7 displays the DBE vs carbon number plots for the O*x* group for the three extrography fractions from the flowline and separator samples. An additional plot (far right) that combines the composition from all the extrography fractions is provided to facilitate sample comparison. We would like to highlight that the peak list and measured peak intensities (abundances) were combined to illustrate the accessed compositional range, without consideration of fraction yields. Renormalization based on fraction yields was not performed, as the focus of this work is on compositional diversity rather than quantification. In Figure 7, the discontinuities observed in the summed composition are likely attributed to nonionized species that remain unseen, possibly due to aggregation during the ionization process. This effect has been described previously by Chacón-Patiño et al. (2018), in studies examining the Boduszynski Continuum Theory using FT-ICR MS.[76] Both samples reveal abundant species with a DBE of 3, which likely correspond to highly abundant carboxylic acids with two saturated rings (naphthenic acids). Such species have been previously observed in samples associated with field problems and tend to be red flags for deposit/fouling challenges.[68,69] In general, the flowline deposit reveals O*x*

https://doi.org/10.1021/acs.energyfuels.4c03528
Energy Fuels XXXX, XXX, XXX−XXX

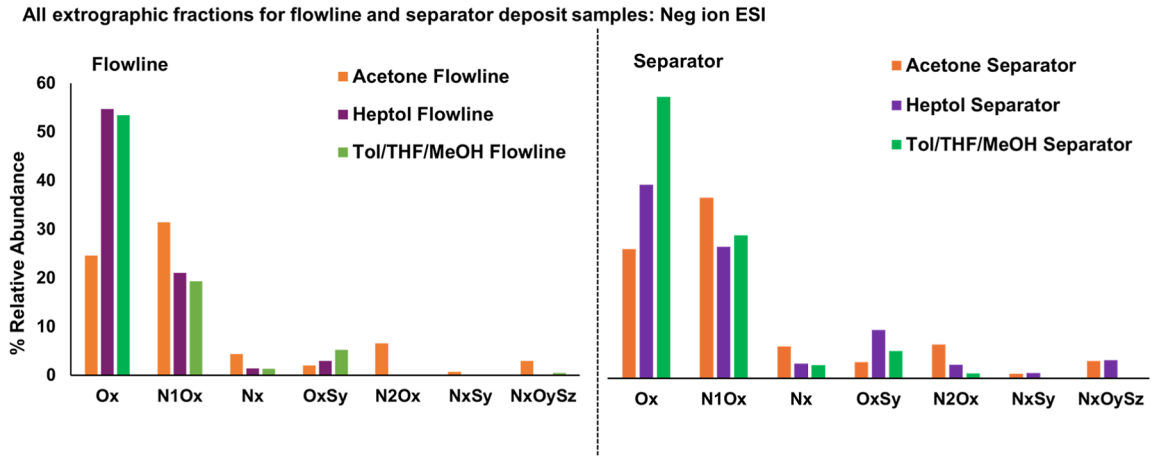

Figure 6. Heteroatom class distributions for the most abundant classes in the acetone, Hep/Tol, and Tol/THF/MeOH extrography fractions in the flowline (left) and separator (right) samples analyzed by (−) ESI 21 T FT-ICR MS.

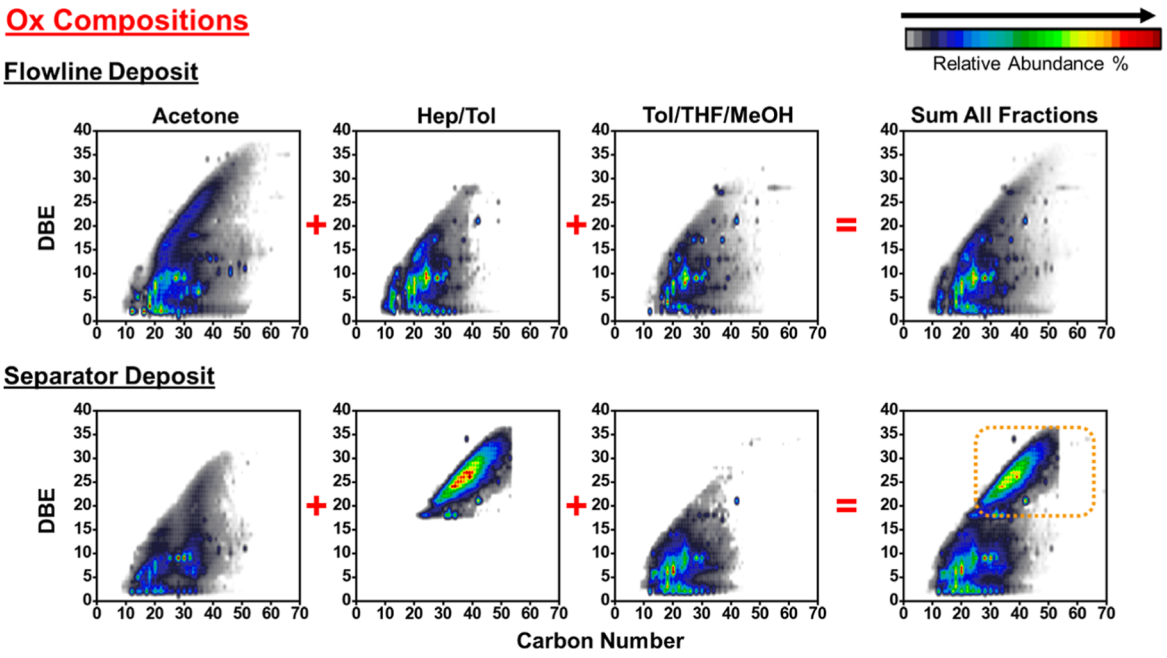

Figure 7. Combined DBE vs carbon number plots for O*x* species (i.e., O_1, O_2, O_3, O_4, and O_5) for the three extrography fractions for the flowline deposit (upper row) and the separator deposit (lower row). The plots to the right combine all molecular formulas detected in the three fractions to facilitate the discussion of results. Strong bimodal compositional nature for separator deposit is highlighted in the summed O*x* species with high-DBE distribution species circled in orange.

species with a lower DBE range in all the extrography fractions. On the other hand, the summed DBE vs C# plot indicates a strong bimodal compositional nature for the separator deposit: the high-DBE distribution (circled in orange) suggests the presence of highly aromatic species with oxygen atoms likely embedded within aromatic cores (e.g., furans and phenols), whereas the low-DBE distribution likely contains a wide diversity of naphthenic acids and combinations of acidic functionalities. Collectively, the data suggest that the separator sample is rich in single-core (island) structural motifs.

Figure 8 features the DBE vs carbon number plots for the NO*x* group for the three extrography fractions from the two samples plus the sum of all assigned compositions for the three extrography fractions (far right). Again, the separator deposit reveals a much higher abundance of species with higher DBE values (or aromaticity). The Hep/Tol fraction from the separator deposit is highly aromatic and lacks low DBE compounds. The plot of the sum of all fractions indicates that the flowline deposit has abundant compositions with DBE below 20. Such prominent homologous series at DBE <20, at high heteroatom contents, detected in the later 2 extrography fractions, point to the highly polar nature of the flowline deposit species.

Figure 9 presents the compositional range for the S*x*O*y* species identified in the extrography fractions from the two deposit samples. Again, the plot to the right combines all the species detected in the three fractions. Both deposit samples reveal S-containing compounds with low DBE values, which are more prominent in the separator deposit and similar to what was observed for the C_5 maltenes. The composition of the S*x*O*y* species matches that of the N*x*O*y* from the Hep/Tol fraction for separator deposit. It reveals highly aromatic species

https://doi.org/10.1021/acs.energyfuels.4c03528
Energy Fuels XXXX, XXX, XXX−XXX

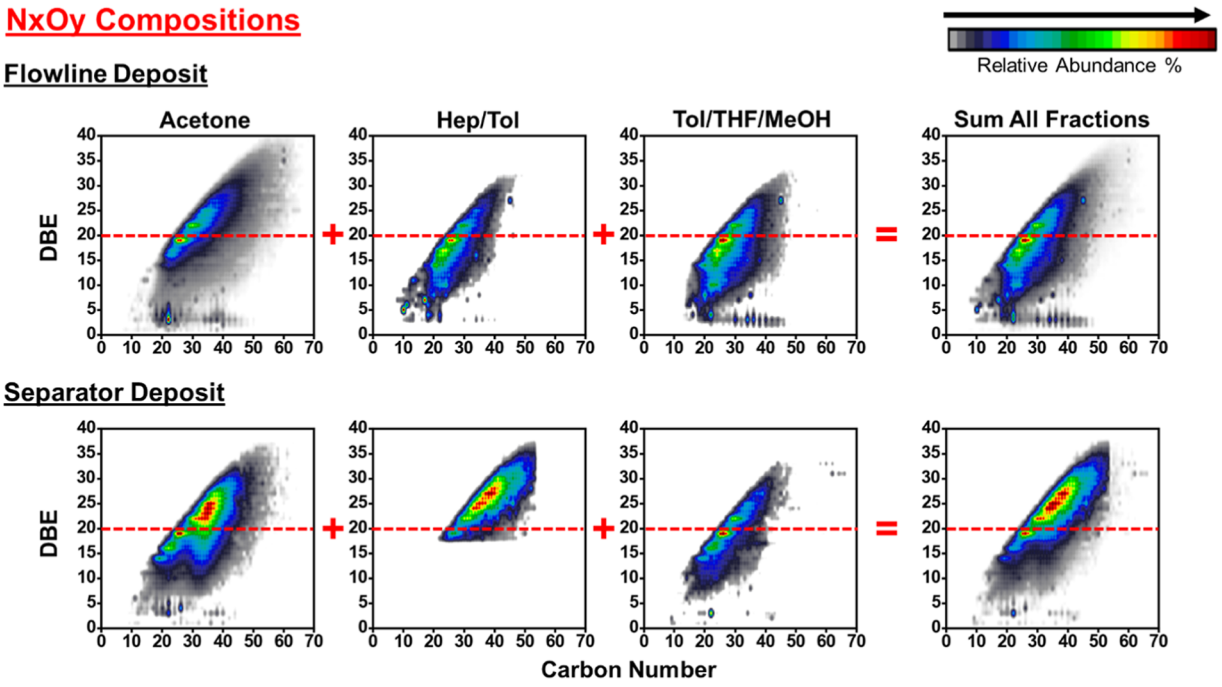

Figure 8. Combined DBE vs carbon number plots for N*x*O*y* species for the three extrography fractions for the flowline deposit (upper row) and the separator deposit (lower row). Plots to the right combine all molecular formulas detected in the three fractions to facilitate the discussion of results.

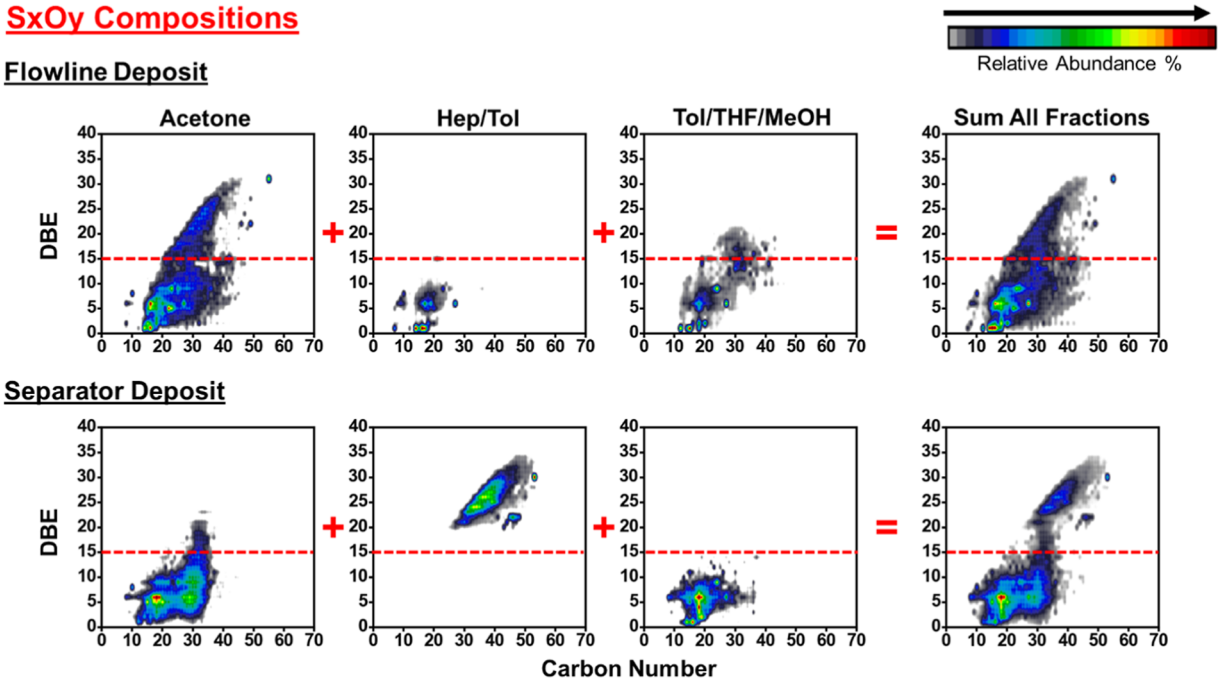

Figure 9. Combined DBE vs carbon number plots for S*x*O*y* species for the three extrography fractions for the flowline deposit (upper row) and the separator deposit (lower row). The plots to the right combine all molecular formulas detected in the three fractions to facilitate the discussion of results.

whose compositional space (DBE and C# range) is consistent with highly aromatic asphaltenes, likely enriched in single-core structural motifs. Conversely, low DBE S*x*O*y* species are apparent in both samples and have been reported in petroleum samples as natural surfactants, potentially naturally occurring sulfonic acids, with high interfacial activities.[68,69]

Discussion of the composition of the whole deposit (APPI), maltenes [(−) ESI], "inbetweeners" [(−) ESI], and each extrographic fraction [(−) ESI] provides an opportunity to point out several trends that could explain the aggregation/deposition behavior of the studied deposits. The general class survey of all deposits via APPI establishes several noteworthy compositional trends. Unsurprisingly, hydrocarbons (HC), nitrogen (N_1), and sulfur (S_1) classes are some of the most abundant classes, but the high relative abundance of the O*x*, NO*x*, and SO*x* species is of particular interest, especially in a

https://doi.org/10.1021/acs.energyfuels.4c03528
Energy Fuels XXXX, XXX, XXX−XXX

deposit sample. Analysis of the maltenes corroborates the APPI results on the whole deposit (abundant pyrrolic N_1 species), HC/S1 classes are absent (due to ionization mode), and establishes the O*x*, NO*x*, and SO*x* species as abundant and polar (given their detection via (−) ESI). Progression to the "inbetweeners" marks a drop in the N_1 abundance as O*x* and NO*x* classes emerge as the most abundant. The extrography fractions continue this trend into the Ace fraction; however, O*x* species overtake the NO*x* species as the most abundant in the later 2 (Hep/Tol and Tol/THF/MeOH) extrography fractions. Collectively, the results point to an increasing abundance of acidic, polar species from the maltenes to the last extrography fraction. Previous works demonstrated that compounds in the Ace fraction are less likely to aggregate when compared to the species in the Hep/Tol and Tol/THF/MeOH fractions.[31,73] Therefore, we hypothesize that even though identical formulas may appear in multiple fractions for both samples, they are most likely isomers that are separated based on structural differences, chemical functionality, polarity, and aggregation tendencies, which contribute to the difference in solubility/extractability.[31]

The dominance of oxygen-containing species in all of the extrography fractions is consistent with previous reports of asphaltene adsorption on polar surfaces. Indeed, high oxygen content correlates with a strong adsorption behavior, whereas sulfur and nitrogen contents do not appear to have a critical role in asphaltene interaction with polar surfaces.[57,75,77−79] Results from the in-depth characterization of acidic species from the two deposit samples from the same crude oil production facility demonstrate that low DBE (low aromaticity) species, considered atypical for asphaltenes, also reside in the asphaltene solubility class and have a significant impact on deposition tendencies.[80] The compositional range of O*x* asphaltene compounds of lower aromaticity that concentrate in the subsea deposit sample is particularly noteworthy. In line with previous reports,[56,80] the data suggests that polyfunctional oxygen- and sulfur-containing acidic species are central to asphaltene aggregation and surface adsorption. The work herein suggests that NO*x* species are of interest as well, most likely due to their oxygen, not nitrogen, chemical functionalities.

Such chemical moieties, with low aromaticity (low DBE), may not fit the conventional description of asphaltenes, traditionally thought to be the most aromatic compounds within the pool of molecules in the crude oil matrix, which aggregate mainly via π-stacking. Such low-DBE species concentrate in the most insoluble/prone-to-precipitate asphaltene subfractions, likely because they aggregate via other intermolecular forces such as hydrogen bonding and acid−base interactions.[56] Both samples reveal abundant species with DBE = 3, which likely correspond to highly abundant carboxylic acids with two saturated rings (naphthenic acids). Such species have been previously observed in samples associated with field problems and tend to be red flags for deposit/fouling challenges.[75,80] We hypothesize that acidic species, such as those identified in this study, might be critical for a model to predict asphaltene deposition. It would be valuable to diligently pursue deposition dynamics of various asphaltene fractions, as has been reported earlier by Lin et al.,[67] to elucidate unique contributions by asphaltene subfractions based on molecular motifs.

4. CONCLUSIONS

Extrographic separation and molecular-level characterization of flowline (subsea) and separator (topside) asphaltene deposits from a GOM field were performed to understand chemical differences between the samples. For the producing field highlighted in this study, asphaltene species that deposit in the flowlines are dissimilar, at the molecular level, to asphaltenes that settle in topside facilities. Therefore, for this producing field, subsea (flowline) deposition and topside (separator) sedimentation have distinct molecular drivers. The flowline deposit is dominated by species with relatively smaller aromatic cores (DBE <15), whereas separator settling featured abundant "larger" aromatic cores (DBE >15). As reported earlier, asphaltenes with "atypical composition", i.e., low DBE but high heteroatom content, appear to be a critical mechanistic driver in deposition. Expanding on these analyses from other fields to discern molecular level dissimilarity between subsea (flowline) and topside (separator) deposits would be a reasonable path forward to further support our finding.

The role of polyfunctional, oxygen-containing species in asphaltene deposition has been previously highlighted, and such species are highly abundant in deposits from problematic oils,[74,78−80] similar to the samples presented in this study. The information gleaned here may help expand our understanding of the chemical drivers of deposition, gravitational settling, and laboratory-to-field correlations and facilitate the improved design of asphaltene inhibitors. Therefore, we suggest continued efforts to understand the molecular composition and the intermolecular forces involved in the deposition of asphaltene species that impact different parts of the production facilities. Moreover, in future work, to further explore the unrecoverable absorbed by the silica gel, we plan to use an asphaltene supersolvent, commonly employed in industrial settings to dissolve difficult asphaltene deposits, to desorb more material for analysis with ESI or APPI FT-ICR MS, and possibly including MALDI. The greater the amount of species remaining adsorbed on the silica gel, the more polar and problematic the sample, indicating a higher risk of deposition challenges.

AUTHOR INFORMATION

Corresponding Author

Priyanka Juyal − *ChampionX LLC, Sugar Land, Texas 77478, United States;* orcid.org/0000-0001-8658-5561; Email: pjuyal@championx.com

Authors

Martha Liliana Chacón-Patiño − *National High Magnetic Field Laboratory and Future Fuels Institute, Florida State University, Tallahassee, Florida 32310, United States; International Joint Laboratory for Complex Matrices Molecular Characterization, IC2MC, TRTG, 76700 Harfleur, France;* orcid.org/0000-0002-7273-5343

Ryan P. Rodgers − *National High Magnetic Field Laboratory and Future Fuels Institute, Florida State University, Tallahassee, Florida 32310, United States; International Joint Laboratory for Complex Matrices Molecular Characterization, IC2MC, TRTG, 76700 Harfleur, France; Université de Pau et des Pays de L'Adour, E2S UPPA, CNRS, IPREM, Institut des Sciences Analytiques et de Physico-chimie pour L'Environnement et Les Materiaux,*

https://doi.org/10.1021/acs.energyfuels.4c03528
Energy Fuels XXXX, XXX, XXX−XXX

Hélioparc 64053 Pau, France; orcid.org/0000-0003-1302-2850

Complete contact information is available at: https://pubs.acs.org/10.1021/acs.energyfuels.4c03528

Notes

The authors declare no competing financial interest.

■ ACKNOWLEDGMENTS

Part of this work was performed at The National MagLab, funded by the National Science Foundation (DMR-2128556) and the State of Florida.

■ REFERENCES

(1) Vargas, F. M. Modeling of Asphaltene Precipitation and Arterial Deposition. Ph.D. Thesis; Rice University: Houston, TX, 2010.

(2) Melendez-Alvarez, A.; Garcia-Bermudes, M.; Tavakkoli, M.; Doherty, R.; Meng, S.; Abdallah, D.; Vargas, F. M. On the evaluation of the performance of asphaltene dispersants. *Fuel* **2016**, *179*, 210−220.

(3) Dickie, J.; Haller, M.; Yen, T. F. Electron Microscopic Investigations on the Nature of Petroleum Asphaltics. *J. Colloid Interface Sci.* **1969**, *29* (3), 475−484.

(4) Mansoori, G. A. A unified perspective on the phase behaviour of petroleum fluids. *Int. J. Oil, Gas Coal Technol.* **2009**, *2* (2), 141−167.

(5) Buckley, J. S. Asphaltene Deposition. *Energy Fuels* **2012**, *26* (7), 4086−4090.

(6) Molina V, D.; Ariza Leon, E.; Chaves-Guerrero, A. Understanding the Effect of Chemical Structure of Asphaltenes on Wax Crystallization of Crude Oils from Colorado Oil Field. *Energy Fuels* **2017**, *31*, 8997−9005.

(7) Eskin, D.; Mohammadzadeh, O.; Akbarzadeh, K.; Taylor, S. D.; Ratulowski, J. Reservoir impairment by asphaltenes: A critical review. *Can. J. Chem. Eng.* **2016**, *94* (6), 1202−1217.

(8) Sjoblom, J.; Hemmingsen, P. V.; Kallevik, H. The Role of Asphaltenes in Stabilizing Water-in-Crude Oil Emulsions. In *Asphaltenes, Heavy Oils, and Petroleomics*; Mullins, O. C., Sheu, E. Y., Hammami, A., Marshall, A. G., Eds.; Springer: New York, NY, 2007; pp 549−588..

(9) Stark, J. L.; Asomaning, S. Crude Oil Blending Effects on Asphaltene Stability in Refinery Fouling. *Pet. Sci. Technol.* **2003**, *21*, 569−579.

(10) Vargas, F. M.; Garcia-Bermudes, M.; Boggara, M.; Punnapala, S.; Abutaqiya, M.; Mathew, N.; Prasad, S.; Khaleel, A.; Al Rashed, M.; Al Asafen, H. On the development of an enhanced method to predict asphaltene precipitation. In *Proc. Annual Offshore Technol. Conf. Paper Number: OTC-25294-MS*: Houston, TX, 2014..

(11) Indo, K.; Ratulowski, J.; Dindoruk, B.; Gao, J.; Zuo, J.; Mullins, O. C. Asphaltene Nanoaggregates Measured in a Live Crude Oil by Centrifugation. *Energy Fuels* **2009**, *23*, 4460−4469.

(12) Mullins, O. C. The Modified Yen Model†. *Energy Fuels* **2010**, *24*, 2179−2207.

(13) Haskett, C. E.; Tartera, M. A Practical Solution to the Problem of Asphaltene Deposits-Hassi Messaoud Field, Algeria. *J. Pet. Technol.* **1965**, *17*, 387−391.

(14) Clementz, D. M. Alteration of Rock Properties by Adsorption of Petroleum Heavy Ends: Implications for Enhanced Oil Recovery. *Paper Number: SPE-10683-MS in at the SPE Enhanced Oil Recovery Symposium*, 1982..

(15) Wang, S.; Civan, F. Modeling Formation Damage by Asphaltene Deposition During Primary Oil Recovery. *J. Energy Resour Technol.* **2005**, *127* (4), 310−317.

(16) Creek, J. L. Freedom of Action in the State of Asphaltenes: Escape from Conventional Wisdom. *Energy Fuels* **2005**, *19*, 1212−1224.

(17) Jamshidnezhad, M. Prediction of Asphaltene Precipitation in an Iranian South Oil Field. In *Canadian International Petroleum Conference*: Calgary, Alberta, 2005..

(18) Alkafeef, S. F.; Al-Medhadi, F.; AL-Shammari, A. D. A Simplified Method to Predict and Prevent Asphaltene Deposition in Oilwell Tubings: Field Case. *SPE Annual Technical Conference and Exhibition*, 2003..

(19) Thawer, R.; Nicoll, D. C. A.; Dick, G. Asphaltene Deposition in Production Facilities. *Eng.* **1990**, *5*, 475−480.

(20) Tuttle, R. N. High-Pour-Point and Asphaltic Crude Oils and Condensates. *J. Pet. Technol.* **1983**, *35*, 1192−1196.

(21) Kokal, S. L.; Sayegh, S. G. Asphaltenes: The Cholesterol of Petroleum. *Society of Petroleum Engineers, the Middle East Oil Show*, **1995**..

(22) Purcell, J. M.; Merdrignac, I.; Rodgers, R. P.; Marshall, A. G.; Gauthier, T.; Guibard, I. Stepwise structural characterization of asphaltenes during deep hydroconversion processes determined by Atmospheric Pressure Photoionization (APPI) Fourier Transform Ion Cyclotron Resonance (FT-ICR) Mass Spectrometry. *Energy Fuels* **2010**, *24*, 2257−2265.

(23) Herod, A. A. Limitations of mass spectrometric methods for the characterization of polydisperse materials. *Rapid Commun. Mass Spectrom.* **2010**, *24*, 2507−2519.

(24) Herod, A. A.; Bartle, K. D.; Morgan, T. J.; Kandiyoti, R. Analytical Methods for Characterizing High-Mass Complex Polydisperse Hydrocarbon Mixtures: An Overview. *Chem. Rev.* **2012**, *112* (7), 3892−3923.

(25) Tavakkoli, M.; Panuganti, S. R.; Taghikhani, V.; Pishvaie, M. R.; Chapman, W. G. Understanding the polydisperse behavior of asphaltenes during precipitation. *Fuel* **2014**, *117*, 206−217.

(26) Rodgers, R. P.; Schaub, T. M.; Marshall, A. G. Petroleomics: Mass spectrometry returns to its roots. *Anal. Chem.* **2005**, *77*, 20 A−27 A.

(27) Strausz, O. P.; Mojelsky, T. W.; Lown, E. M. The molecular structure of asphaltene: an unfolding story. *Fuel* **1992**, *71*, 1355−1363.

(28) Mullins, O. C.; Sabbah, H.; Eyssautier, J.; Pomerantz, A. E.; Barré, L.; Andrews, A. B.; Ruiz-Morales, Y.; Mostowfi, F.; McFarlane, R.; Goual, L.; Lepkowicz, R.; Cooper, T.; Orbulescu, J.; Leblanc, R. M.; Edwards, J.; Zare, R. N. Advances in Asphaltene Science and the Yen-Mullins Model. *Energy Fuels* **2012**, *26* (7), 3986−4003.

(29) Alvarez-Ramírez, F.; Ruiz-Morales, Y. Island versus archipelago architecture for asphaltenes: polycyclic aromatic hydrocarbon dimer theoretical studies. *Energy Fuels* **2013**, *27*, 1791−1808.

(30) Chacón-Patiño, M. L.; Rowland, S.; Rodgers, R. P. Advances in Asphaltene Petroleomics. Part 2: Selective Separation Method That Reveals Fractions Enriched in Island and Archipelago Structural Motifs by Mass Spectrometry. *Energy Fuels* **2018**, *32*, 314−328.

(31) Chacón-Patiño, M. L.; Rowland, S.; Rodgers, R. P. Advances in Asphaltene Petroleomics. Part 1: Asphaltenes Are Composed of Abundant Island and Archipelago Structural Motifs. *Energy Fuels* **2017**, *31*, 13509−13518.

(32) McKenna, A. M.; Chacón-Patiño, M. L.; Weisbrod, C. R.; Blakney, G. T.; Rodgers, R. P. Molecular-Level Characterization of Asphaltenes Isolated from Distillation Cuts. *Energy Fuels* **2019**, *33*, 2018−2029.

(33) McKenna, A. M.; Donald, L. J.; Fitzsimmons, J. E.; Juyal, P.; Spicer, V.; Standing, K. G.; Marshall, A. G.; Rodgers, R. P. Heavy Petroleum Composition. 3. Asphaltene Aggregation. *Energy Fuels* **2013**, *27*, 1246−1256.

(34) Juyal, P.; Yen, A. T.; Rodgers, R. P.; Allenson, S. J.; Wang, J.; Creek, J. Compositional Variations between Precipitated and Organic Solid Deposition Control (OSDC) Asphaltenes and the Effect of Inhibitors on Deposition by Electrospray Ionization Fourier Transform Ion Cyclotron Resonance (FT-ICR) Mass Spectrometry. *Energy Fuels* **2010**, *24*, 2320−2326.

(35) Nyadong, L.; Lai, J.; Thompsen, C.; LaFrancois, C.; Cai, X.; Song, C.; Wang, J.; Wang, W. High-field Orbitrap Mass Spectrometry

and Tandem Mass Spectrometry for Molecular Characterization of Asphaltenes. *Energy Fuels* **2018**, *32* (1), 294−305.
(36) Silva, L. C.; Dávila, J. V.; Roque, J. V.; et al. Structural characterization of asphaltenes enriched in Island and archipelago motifs by LDI (+)FT-ICR MS, Structural characterization of asphaltenes enriched in Island and archipelago motifs by LDI (+) FT-ICR MS. *Braz. J. Chem. Eng.* **2023**, *41*, 633−642.
(37) Juyal, P.; Enayat, S.; Lucente-Schultz, R.; Li, Q.; Karimipour, M.; Tavakkoli, M.; Cao, T.; Yen, A.; Russell, C.; Vargas, F. M. Case Study: Investigation of the performance of an asphaltene inhibitor in the laboratory and the field. *Energy Fuels* **2022**, *36* (4), 1825−1831.
(38) Rezaee, S.; Tavakkoli, M.; Doherty, R.; Vargas, F. M. A New Experimental Method for a Fast and Reliable Quantification of Saturates, Aromatics, Resins, and Asphaltenes in Crude Oils. *Pet. Sci. Technol.* **2020**, *38* (21), 955−961.
(39) Enayat, S.; Rajan Babu, N.; Kuang, J.; Rezaee, S.; Lu, H.; Tavakkoli, M.; Wang, J.; Vargas, F. M. On the Development of Experimental Methods to Determine the Rates of Asphaltene Precipitation, Aggregation, and Deposition. *Fuel* **2020**, *260*, 116250.
(40) Khaleel, A. T.; Sisco, C. J.; Tavakkoli, M.; Vargas, F. M. An Investigation of the Effect of Asphaltene Polydispersity on Asphaltene Precipitation and Deposition Tendencies. *Energy Fuels* **2022**, *36* (16), 8799−8808.
(41) Tavakkoli, M.; Grimes, M. R.; Liu, X.; Garcia, C. K.; Correa, S. C.; Cox, Q. J.; Vargas, F. M. Indirect Method: A Novel Technique for Experimental Determination of Asphaltene Precipitation. *Energy Fuels* **2015**, *29* (5), 2890−2900.
(42) Smith, D. F.; Podgorski, D. C.; Rodgers, R. P.; Blakney, G. T.; Hendrickson, C. L. 21 Tesla FT-ICR Mass Spectrometer for Ultrahigh-Resolution Analysis of Complex Organic Mixtures. *Anal. Chem.* **2018**, *90* (3), 2041−2047.
(43) Hendrickson, C. L.; Quinn, J. P.; Kaiser, N. K.; Smith, D. F.; Blakney, G. T.; Chen, T.; Marshall, A. G.; Weisbrod, C. R.; Beu, S. C. 21 Tesla Fourier Transform Ion Cyclotron Resonance Mass Spectrometer: A National Resource for Ultrahigh Resolution Mass Analysis. *J. Am. Soc. Mass Spectrom.* **2015**, *26*, 1626−1632.
(44) Kaiser, N. K.; Savory, J. J.; Hendrickson, C. L. Controlled Ion Ejection from an External Trap for Extended m/z Range in FT-ICR Mass Spectrometry. *J. Am. Soc. Mass Spectrom.* **2014**, *25*, 943−949.
(45) Kaiser, N. K.; McKenna, A. M.; Savory, J. J.; Hendrickson, C. L.; Marshall, A. G. Tailored Ion Radius Distribution for Increased Dynamic Range in FT-ICR Mass Analysis of Complex Mixtures. *Anal. Chem.* **2013**, *85*, 265−272.
(46) Chen, T.; Beu, S. C.; Kaiser, N. K.; Hendrickson, C. L. Note: Optimized circuit for excitation and detection with one pair of electrodes for improved Fourier transform ion cyclotron resonance mass spectrometry. *Rev. Sci. Instrum.* **2014**, *85* (6), 066107.
(47) Boldin, I. A.; Nikolaev, E. N. Fourier transform ion cyclotron resonance cell with dynamic harmonization of the electric field in the whole volume by shaping of the excitation and detection electrode assembly. *Rapid Commun. Mass Spectrom.* **2011**, *25*, 122−126.
(48) Blakney, G. T.; Hendrickson, C. L.; Marshall, A. G. Predator data station: A fast data acquisition system for advanced FT-ICR MS experiments. *Int. J. Mass Spectrom.* **2011**, *306*, 246−252.
(49) Savory, J. J.; Kaiser, N. K.; McKenna, A. M.; Xian, F.; Blakney, G. T.; Rodgers, R. P.; Hendrickson, C. L.; Marshall, A. G. Parts-per-billion Fourier transform ion cyclotron resonance mass measurement accuracy with a "walking" calibration equation. *Anal. Chem.* **2011**, *83*, 1732−1736.
(50) Corilo, Y. E. *PetroOrg. Software*; Florida State University, Omics LLC: Tallahassee, FL, 2014.
(51) Glattke, T. J.; Chacón-Patiño, M. L.; Marshall, A. G.; Rodgers, R. P. Molecular Characterization of Photochemically Produced Asphaltenes via Photooxidation of Deasphalted Crude Oils. *Energy Fuels* **2020**, *34* (11), 14419−14428.
(52) McKenna, A. M.; Marshall, A. G.; Rodgers, R. P. Heavy Petroleum Composition. 4. Asphaltene Compositional Space. *Energy Fuels* **2013**, *27*, 1257−1267.
(53) Itoh, N.; Aoyagi, Y.; Yarita, T. Optimization of the Dopant for the Trace Determination of Polycyclic Aromatic Hydrocarbons by Liquid Chromatography/Dopant-Assisted Atmospheric-Pressure Photoionization/Mass Spectrometry. *J. Chromatogr. A* **2006**, *1131*, 285−288.
(54) Robb, D. B.; Covey, T. R.; Bruins, A. P. Atmospheric Pressure Photoionization: An Ionization Method for Liquid Chromatography-Mass Spectrometry. *Anal. Chem.* **2000**, *72*, 3653−3659.
(55) Rogel, E.; Moir, M.; Witt, M. Atmospheric Pressure Photoionization and Laser Desorption Ionization Coupled to Fourier Transform Ion Cyclotron Resonance Mass Spectrometry To Characterize Asphaltene Solubility Fractions: Studying the Link between Molecular Composition and Physical Behavior. *Energy Fuels* **2015**, *29*, 4201−4209.
(56) Gray, M.; Tykwinski, R.; Stryker, J.; Tan, X. Supramolecular Assembly Model for Aggregation of Petroleum Asphaltenes. *Energy Fuels* **2011**, *25* (7), 3125−3134.
(57) Andreatta, G.; Bostrom, N.; Mullins, O. C. High-Q ultrasonic determination of the critical nanoaggregate concentration of asphaltenes and the critical micelle concentration of standard surfactants. *Langmuir* **2005**, *21*, 2728−2736.
(58) Pomerantz, A. E.; Hammond, M. R.; Morrow, A. L.; Mullins, O. C.; Zare, R. N. Two-step laser mass spectrometry of asphaltenes. *J. Am. Chem. Soc.* **2008**, *130*, 7216−7217.
(59) Chacón-Patiño, M. L.; Neumann, A.; Rüger, C. P.; Bomben, P. G.; Friederici, L.; Zimmermann, R.; Frank, E.; Kreis, P.; Buchmeiser, M. R.; Gray, M. Chemistry and Properties of Carbon Fiber Feedstocks from Bitumen Asphaltenes. *Energy Fuels* **2023**, *37* (7), 5341−5360.
(60) Chacón-Patiño, M. L.; Heshka, N.; Alvarez-Majmutov, A.; Hendrickson, C. L.; Rodgers, R. P. Molecular characterization of remnant polarizable asphaltene fractions upon bitumen upgrading and possible implications in petroleum viscosity. *Energy Fuels* **2022**, *36* (14), 7542−7557.
(61) Rodgers, R. P.; Mapolelo, M. M.; Robbins, W. K.; Chacón-Patiño, M. L.; Putman, J. C.; Niles, S. F.; Rowland, S. M.; Marshall, A. G. Combating selective ionization in the high resolution mass spectral characterization of complex mixtures. *Faraday Discuss.* **2019**, *218*, 29−51.
(62) Chacón-Patiño, M. L.; Nelson, J.; Rogel, E.; Hench, K.; Poirier, L.; Lopez-Linares, F.; Ovalles, C. Vanadium and nickel distributions in selective-separated n-heptane asphaltenes of heavy crude oils. *Fuel* **2022**, *312* (2), 122939.
(63) Pomerantz, A. E.; Hammond, M. R.; Morrow, A. L.; Mullins, O. C.; Zare, R. N. Asphaltene Molecular-Mass Distribution Determined by Two-Step Laser Mass Spectrometry. *Energy Fuels* **2009**, *23*, 1162−1168.
(64) Subramanian, S.; Simon, S.; Gao, B.; Sjoblom, J. Asphaltene fractionation based on adsorption onto calcium carbonate: Part 1. Characterization of sub-fractions and QCM-D measurements. *J. Colloids Surf., A* **2016**, *495*, 136−148.
(65) Subramanian, S.; Sorland, G. H.; Simon, S.; Xu, Z.; Sjoblom, J. Asphaltene fractionation based on adsorption onto calcium carbonate: Part 2. Self-association and aggregation properties. *J. Colloids Surf., A* **2017**, *514*, 79−90.
(66) Nascimento, P. T. H.; Santos, A. F.; Yamamoto, C. I.; Tose, L. V.; Barros, E. V.; Gonçalves, G. R.; Freitas, J. C. C.; Vaz, B. G.; Romão, W.; Scheer, A. P. Fractionation of Asphaltene by Adsorption onto Silica and Chemical Characterization by Atmospheric Pressure Photoionization Fourier Transform Ion Cyclotron Resonance Mass Spectrometry, Fourier Transform Infrared Spectroscopy Coupled to Attenuated Total Reflectance, and Proton Nuclear Magnetic Resonance. *Energy Fuels* **2016**, *30*, 5439−5448.
(67) Lin, Y. J.; Cao, T.; Chacón-Patiño, M. L.; Rowland, S. M.; Rodgers, R. P.; Yen, A. T.; Biswal, S. L. Microfluidic Study of the Deposition Dynamics of Asphaltene Subfractions Enriched with Island and Archipelago Motifs. *Energy Fuels* **2019**, *33*, 1882−1891.
(68) Clingenpeel, A. C.; Rowland, S. M.; Corilo, Y. E.; Zito, P.; Rodgers, R. P. Fractionation of Interfacial Material Reveals a

https://doi.org/10.1021/acs.energyfuels.4c03528
Energy Fuels XXXX, XXX, XXX−XXX

Continuum of Acidic Species That Contribute to Stable Emulsion Formation. *Energy Fuels* **2017**, *31* (6), 5933−5939.
(69) Jarvis, J. M.; Robbins, W. K.; Corilo, Y. E.; Rodgers, R. P. Novel method to isolate interfacial material. *Energy Fuels* **2015**, *29* (11), 7058−7064.
(70) Jonker, M. T. O.; Koelmans, A. A. Extraction of polycyclic aromatic hydrocarbons from soot and sediment: solvent evaluation and implications for sorption mechanism. *Environ. Sci. Technol.* **2002**, *36*, 4107−4113.
(71) Barnabas, I. J.; Dean, J. R.; Fowlis, I. A.; Owen, S. P. Extraction of polycyclic aromatic hydrocarbons from highly contaminated soils using microwave energy. *Analyst* **1995**, *120*, 1897−1904.
(72) Rogel, E.; Ovalles, C.; Moir, M. Asphaltene Chemical Characterization as a Function of Solubility: Effects on Stability and Aggregation. *Energy Fuels* **2012**, *26*, 2655−2662.
(73) Buenrostro-Gonzalez, E.; Groenzin, H.; Lira-Galeana, C.; Mullins, O. C.; Mullins, O. C. The Overriding Chemical Principles that Define Asphaltenes. *Energy Fuels* **2001**, *15* (4), 972−978.
(74) Groenzin, H.; Mullins, O. C.; Eser, S.; Mathews, J.; Yang, M.-G.; Jones, D. Molecular Size of Asphaltene Solubility Fractions. *Energy Fuels* **2003**, *17*, 498−503.
(75) Zeng, H.; Tessarolo, N.; Gonzalez, D. L.; Gramin, P.; Wicking, C.; Pietrobon, M. Sticky molecules" on rock surface might play an important role in formation damage due to asphaltene deposition. *Fuel* **2020**, *277*, 117983.
(76) Chacón-Patiño, M. L.; Rowland, S. M.; Rodgers, R. P. The Compositional and Structural Continuum of Petroleum from Light Distillates to Asphaltenes: The Boduszynski Continuum Theory as Revealed by FT-ICR Mass Spectrometry. *ACS Symp. Ser.* **2018**, *1282*, 113−171.
(77) Adams, J. J. Asphaltene Adsorption, a Literature Review. *Energy Fuels* **2014**, *28*, 2831−2856.
(78) Wang, S.; Liu, Q.; Tan, X.; Xu, C.; Gray, M. Study of asphaltene adsorption on kaolinite by X-ray photoelectron spectroscopy and time-of-flight secondary ion mass spectroscopy. *Energy Fuels* **2013**, *27*, 2465−2473.
(79) Marczewski, A.; Szymula, M. Adsorption of asphaltenes from toluene on mineral surface. *Colloids Surf., A* **2002**, *208*, 259−266.
(80) Chacón-Patiño, M. L.; Smith, D. F.; Hendrickson, C. L.; Marshall, A. G.; Rodgers, R. P. Advances in Asphaltene Petroleomics. Part 4. Compositional Trends of Solubility Subfractions Reveal that Polyfunctional Oxygen-Containing Compounds Drive Asphaltene Chemistry. *Energy Fuels* **2020**, *34*, 3013−3030.

https://doi.org/10.1021/acs.energyfuels.4c03528
Energy Fuels XXXX, XXX, XXX−XXX